Full-field Strain Methods for Investigating Failure Mechanisms in Triaxial Braided Composites

Justin D. Littell
The University of Akron, Akron, OH 44325, USA
Justin.D.Littell@nasa.gov

Wieslaw K. Binienda
The University of Akron, Akron, OH 44325, USA
wbinienda@uakron.edu

Robert K. Goldberg
NASA Glenn Research Center, Cleveland OH 44135, USA
Robert.K.Goldberg@nasa.gov

Gary D. Roberts
NASA Glenn Research Center, Cleveland OH 44135, USA
Gary.D.Roberts@nasa.gov

Abstract

Composite materials made with triaxial braid architecture and large tow size carbon fibers are beginning to be used in many applications, including composite aircraft and engine structures. Recent advancements in braiding technology have led to commercially viable manufacturing approaches for making large structures with complex shape. Although the large unit cell size of these materials is an advantage for manufacturing efficiency, the fiber architecture presents some challenges for materials characterization, design, and analysis. In some cases, the static load capability of structures made using these materials has been higher than expected based on material strength properties measured using standard coupon tests. A potential problem with using standard tests methods for these materials is that the unit cell size can be an unacceptably large fraction of the specimen dimensions. More detailed investigation of deformation and failure processes in large unit cell size triaxial braid composites is needed to evaluate the applicability of standard test methods for these materials and to develop alternative testing approaches. In recent years, commercial equipment has become available that enables digital image correlation to be used on a more routine basis for investigation of full field 3D deformation in materials and structures. In this paper, some new techniques that have been developed to investigate local deformation and failure using digital image correlation techniques are presented. The methods were used to measure both local and global strains during standard straight-sided coupon tensile tests on composite materials made with 12 and 24 k yarns and a 0/+60/-60 triaxial braid architecture. Local deformation and failure within fiber bundles was observed, and this local failure had a significant effect on global stiffness and strength. The matrix material had a large effect on local damage initiation for the two matrix materials used in this investigation. Premature failure in regions of the unit

cell near the edge of the straight-sided specimens was observed for transverse tensile tests in which the braid axial fibers were perpendicular to the specimen axis and the bias fibers terminated on the cut edges in the specimen gage section. This edge effect is one factor that could contribute to a measured strength that is lower than the actual material strength in a structure without edge effects.

Introduction

Composite materials made with triaxial braid architecture and large tow size carbon fibers are beginning to be used in many applications, including composite aircraft and engine structures. Recent advancements in braiding technology have led to commercially viable manufacturing approaches for making large structures with complex shape. Although the large unit cell size of these materials is an advantage for manufacturing efficiency, the fiber architecture presents some challenges for materials characterization, design, and analysis. In some cases, the static load capability of structures made using these materials has been higher than expected based on material strength properties measured using standard coupon tests. Existing composite test methods (ASTM, 2006) and composite material databases (MIL-HDBK-17, 2002; FAA, 2003; Tomblin, 2001) have been developed primarily for angle-ply and/or fabric laminates. There has been some research conducted and data generated specifically on braided composite materials. Masters et al. (Masters, 1993; Masters, Feb. 1996; Masters, Sept. 1996; Masters, 1996) have proposed guidelines for strain gage sizes and specimen widths for braided composites. Optical measurement techniques have been used to measure both local and global strain in test specimens. Using Moiré interferometry Masters (Masters Feb. 1996), noticed a significant amount of strain heterogeneity on the surface of composite specimens. Tsotsis examined strain concentrations around holes in open-hole tension specimens (Tsotsis, 2006). Gliesche (Gliesche, 2005) used optical measurement techniques to obtain strains for calculating global material properties. More detailed investigations of the local strain effects noted in these previous investigations is needed, particularly for large unit cell size architectures where the unit cell is a large fraction of specimen dimensions. In recent years, commercial equipment has become available that enables digital image correlation to be used on a more routine basis for investigation of full field 3D deformation in materials and structures. In this paper, some new techniques that have been developed to investigate local deformation and failure using digital image correlation techniques are presented. Some preliminary results are presented for the application of these techniques to measure strain during tensile tests using standard straight-sided coupons.

Experimental Methods

Materials

Composite panels were fabricated by the resin transfer molding (RTM) process using triaxial braided preforms. A high strength, standard modulus carbon fiber (T700S from Toray) was used as the reinforcement. Manufacturer properties for the T700S fiber are shown in Table 1.

	Tensile strength, (MPa)	Young's modulus, (Gpa)	Failure strain, (%)	Density
Toray T700s Fiber	4900	230	2.1	1.80 g/cm^3

Table 1. Fiber Properties.

Two 350 °F cure epoxy resin systems (CYCOM® PR520 and 5208 from Cytec) were used. CYCOM® PR520 is a one part toughened resin specifically designed for resin transfer molding with a recommended cure temperature of 179 ^{o}C. 5208 is a one part untoughened epoxy with a recommended cure temperature of 177 ^{o}C. Table 2 lists manufacturer properties for each resin. A toughened resin and an untoughened resin were selected in order to explore the potential role of matrix toughening on the initiation of local failure within the composite unit cell.

	Tensile strength, (MPa)	Young's modulus, (Gpa)	Failure strain, (%)	Density
Cytec CYCOM® PR520	82	4.00	NA	1.256g/cm^3
Cytec 5208	50	3.8	NA	1.265g/cm^3

Table 2. Resin Properties.

2'X2'X0.125" composite panels were fabricated in an enclosed RTM mold by North Coast Composites using braided preforms from A&P Technology. Figure 1 shows an example of the braided material and the size of a unit cell. The preform architecture was 0^{o}/+60^{o}/-60^{o} with 24 k tows in the axial (0°) direction and 12 k tows in the bias (+60° and -60°) directions. The number of 24 k tows in the axial direction was half that of the 12 k tows in the bias directions, so the total fiber volume in each direction was the same. As a result the stiffness of the 0^{o}/+60^{o}/-60^{o} laminate, and each ply within the laminate, is expected to be quasi-isotropic. The preform was supplied in the form of a braided tube. Three layers of the flattened tube (six total plies) were placed in the RTM mold with 0^{o} (axial) fibers aligned, and resin was injected and cured under conditions specified by the resin manufacturer. The nominal fiber volume was calculated to be 56%, and the actual fiber volume was measured by the acid digestion technique on samples from a representative panel for each material system. The fiber volume of a T700S/ PR520 composite panel was measured to be 55.9±0.18%, and the fiber volume of a T700S/5208 panel was measured to be 53.0±3.3%.

Specimen Geometries

Test specimens were cut from the panels using an abrasive waterjet technique. Straight sided tensile test specimens were prepared and tested according to the standard ASTM D-3039 test method. The specimen length was 12" and the width was 1.409". These dimensions were chosen so that the width contained at least two unit cells and the length conformed with allowable length to width ratios in ASTM D-3039 standard. Specimens were cut with axial fibers aligned with the axis of the specimen to yield axial tensile properties and with axial fibers aligned perpendicular to the axis of the specimen to yield transverse tensile properties.

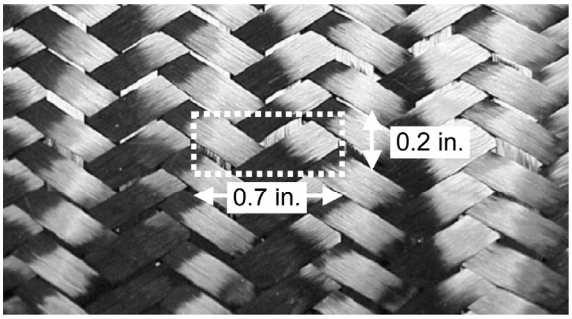

Figure 1. An example 2D triaxial composite braid.

Test Equipment

All specimens were tested in an MTS 858 axial-torsional test machine. Tests were conducted under displacement control at rates of 0.025 in./min. Strain was measured by the digital image correlation technique using a commercial system developed by GOM (GOM, 2008). Stress strain curves were generated using the strain measurements and a synchronized load input from the MTS machine. The optical measurement technique is similar to the one described in Littell et al. (Littell, In Pub). Two cameras are connected to a computer equipped with software capable of pattern recognition. After a calibration procedure is completed, a test specimen with a speckle pattern applied to the surface is placed within the calibrated space. The position of any point on the surface of a test specimen can then be determined by the software using the stereo images of the specimen. The strain is then calculated from surface displacements measured at specified time intervals during a test.

Results

Global stress-strain data

Figure 2 shows an example of the full field axial strain distribution acquired using the optical measurement system during an axial tension test. The field of view captures the entire 1.409 in. specimen width and approximately 2 in. of the specimen height. The local strains induced by the (0/+60/-60) braid architecture are apparent. The average, or global, strain in any region can be determined by selecting specific points on the specimen and tracking the displacement of these points during the test. For this work, global strains were calculated using points that were initially about 0.75 in. apart. The locations of these points are shown in Figure 2. A distance of 0.75 in. is consistent with guidelines proposed by Masters (Masters, 2003). Global strains in the axial and transverse directions were used to calculate a global Poisson ratio.

Representative stress versus global strain curves are shown for the two materials systems in Figures 3 and 4.

Material modulus was calculated by taking the slopes of the stress-strain curve in the region from 0.0 to 0.2% strain. Since a data point was not collected at exactly 0.2% strain, the data point collected closest to 0.2% strain was used for the upper limit. A

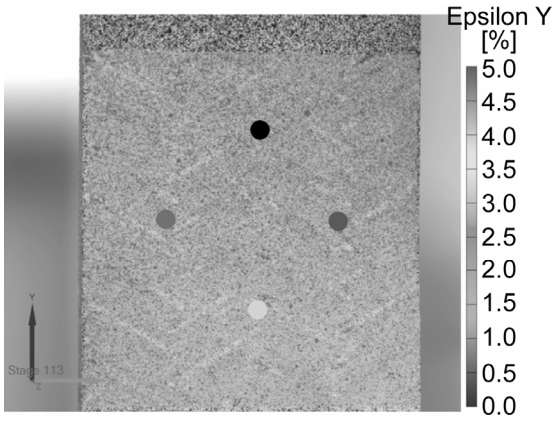

Figure 2. Typical full field strain distribution and point map used for global strain calculations.

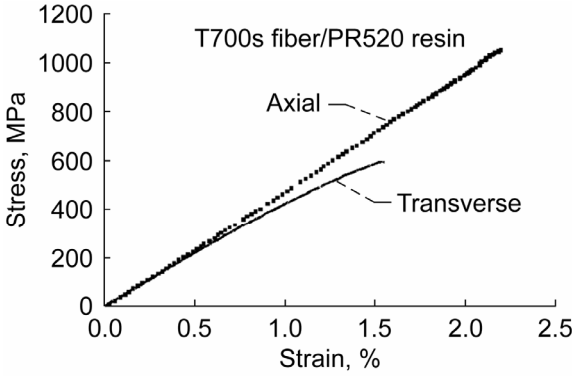

Figure 3. Stress versus strain for T700s fiber/ PR520 material system.

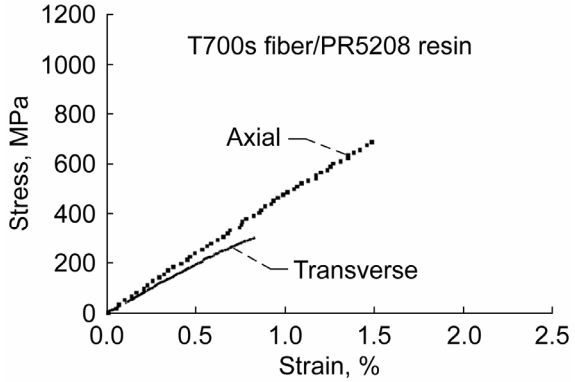

Figure 4. Stress versus strain for T700s fiber/ PR5208 material system.

global Poisson ratio was calculated using the strains in the axial and transverse directions. Table 3 shows the moduli, strengths, failure strains and Poisson ratios for the two material systems. A minimum of five tests were conducted to obtain average values, and the error limits shown are one standard deviation.

Material (fiber /resin)	Axial direction			Transverse direction			
	Strength, (MPa)	Young's modulus, (GPa)	Failure strain, (%)	Strength, (MPa)	Young's modulus, (GPa)	Failure strain, (%)	Poisson ratio
T700s /PR520	1035±34	47.6±1.1	2.16±0.09	599±3	42.8±1.6	1.68±0.19	0.31±0.02
T700s /5208	693±46	47.0±1.0	1.5±0.09	310±15	41.4±4.5	0.85±0.05	0.29±0.03

Table 3. Material Properties for the two material systems.

The axial stress-strain curve for T700S/PR520 are linear until failure, while the curve for T700S/5208 shows a slight nonlinearity beginning at about 1.2%. The axial moduli are nearly equal for the two material systems. The axial failure strain for T700S/PR520 is 2.16%, which is close to the ultimate fiber failure strain of 2.1% shown in Table 1. However, the axial failure strain for T700S/5208 is only 1.5%, which is 35% less than the ultimate fiber strain. The reduced strain capability for the T700S/5208 system also results in a reduced failure strength. A possible explanation

for the differences in material behavior is that local failure occurs earlier in an untoughened system and that this failure leads to nonlinear global behavior, localized stress concentrations, and early failure of the axial tows in the triaxial braid. The digital image correlation techniques reported in this paper were developed to investigate these potential local failure events.

In the transverse direction, the matrix plays an even more important role in material response because there are no continuous fibers that extend between the two gripped areas of the straight-sided test specimen. As a result, load transfer must occur through matrix material and the fiber/matrix interface. Compared to the axial stress-strain curves, the transverse curves of both materials show more nonlinearity, have lower strains to failure, and have a slightly lower initial slope (i.e., lower moduli in Table 3). The nonlinearity of the transverse stress-strain curves could be a consequence of local damage occurring within a unit cell, either within the matrix or at the fiber/matrix interface. The reduced strain to failure could be a result of this local damage leading to local stress concentrations. The reduced modulus could also be a result of local damage occurring at low strains, but it is also possible that the material is not exactly quasi-isotropic. Microscopic analysis of specimens from tensile tests conducted to various levels of strain could be used to better identify the initiation and growth of local failures. However, it would be more efficient if this type of information could be obtained during the test. The remainder of this paper describes optical methods that can be applied during a test to obtain much of this microscopic information needed for failure analysis

Local deformation and failure

An indication of the occurrence of local strain concentrations and the effect of braid architecture on the strain field was shown in Figure 2. In order to more accurately relate the strain field to specific features of the specimen, overlay techniques were developed to map the strain field onto an image of the specimen. An example of the method is shown in Figure 5 using a T700S/PR520 axial tensile specimen.

Figure 5A shows a digital image of the specimen before the surface is painted with the speckle pattern that is needed to measure strain by the digital image correlation method. After the specimen is painted with a speckle pattern it is mounted in the tensile test apparatus. The deformation of the speckle pattern is then tracked by taking a sequence of stereo images during a tensile test. The cameras used for these measurements and the software used for post processing of the images to obtain 3D deformation from the stereo images are part of the full commercial instrumentation system used for this work. Figure 5B shows the post processed strain data obtained by digital image correlation mapped onto the deformed speckle pattern using images that were taken when the specimen was loaded to 2.19% strain. Figure 5C shows the post processed strain data only. An image overlay is made in several steps using an image editing program. First, the image in Figure 5B is mapped onto the image in Figure 5A by matching visible fiber locations. Then the image in Figure 5C is mapped onto the combined images from Figure 5A and 5B by matching strain results. The image from Figure 5B is then removed, leaving the final overlay of the image from Figure 5C over the image from Figure 5A. Finally, the opacity is reduced for the image in the overly that was obtained from Figure 5C so that the fibers in the image that was obtained from Figure 5A are visible. Figure 6 shows the final overlay obtained from the images in Figure 5.

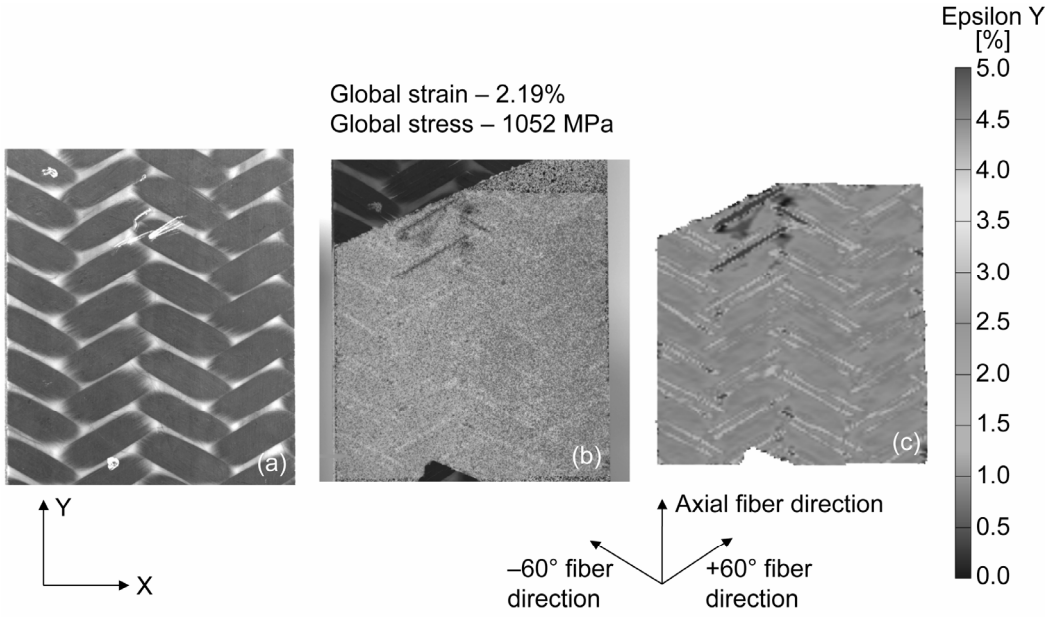

Figure 5. Development of the overlay technique for the T700s/fiber/PR520 resin material system.

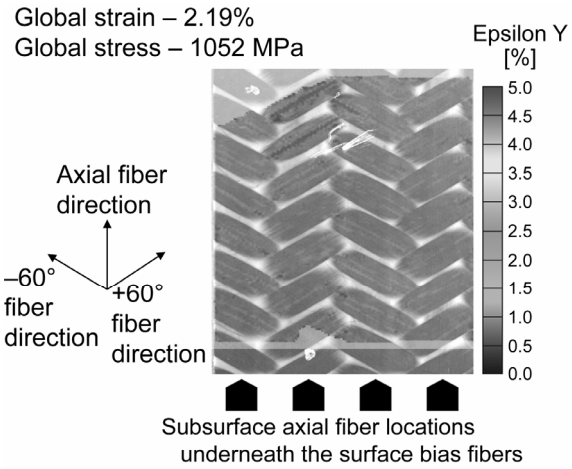

Figure 6. Axial strain overlay on an axial specimen in the T700s fiber/PR520 resin material system.

The overlay in Figure 6 shows an accurate mapping of localized strain concentrations onto the surface braid architecture in the specimen. This is useful for viewing the occurrence and growth of strain concentrations before there is visible damage. However, the overlay technique distorts the color pattern, so Figures 5C and 6 must be used in combination in order to determine the location and magnitude of strain concentrations. As an example, the areas between the fiber tows of the specimen appear to be white in Figure 6 because the result of the overlay process emphasizes the white from the digital image of the surface rather than the color pattern from the strain map. Figure 6 alone might suggest that the strain in these matrix regions is much different from the strain in the surrounding fiber bundles. However, Figure 5C indicates that such a strain discontinuity does not exist. As another example, Figure 5C indicates that there are strain concentrations with direction and periodicity

equal to that of the surface bias fibers in the braid architecture. Using Figure 6C alone, it might appear that the regions of high strain concentration are at the edges of the bias fiber bundles. However, Figure 6 clearly shows that the regions of strain concentration are splits within fiber bundles rather than cracks at the edges of the fiber bundles. Data of the type shown in Figure 5C can be used to get a quantitative threshold for damage initiation within fiber bundles. This information is useful for materials evaluation and also provides in-situ material failure properties that could be used in analysis. Work in these areas is ongoing but is beyond the scope of this paper. In Figures 5 and 6, only the surface bias fibers are visible. The black arrows at the bottom of Figure 6 indicate the approximate locations and widths of subsurface axial fibers in an axial tensile test. Transverse loading is discussed below. Although these subsurface axial fibers are not directly visible, load is transferred from these fibers to the surface bias fibers and resin. As a result, the effect of subsurface damage in these fibers can sometimes be visible in the surface strain field. There is no evidence of this effect in Figure 6, but this effect is more prominent for the transverse tensile test results discussed below.

In a transverse tensile test the axial fibers in the braid are oriented perpendicular to the direction of the applied load. An example of an overlay from a transverse tensile test is shown in Figure 7.

There is little splitting within the bias fiber tows. However, there are many small horizontal red lines indicating high strain regions in the surface matrix material located between the bias fibers and above subsurface axial tows. These localized high strain regions are an indication of transverse splitting in the subsurface axial tows. Figure 8 shows the effect of these subsurface axial fiber splits during a transverse tensile test on the T700S/PR520 material at a global strain of 1.73%.

The circled area in Figure 8 shows the localized high strain regions (red horizontal lines) that occur in the surface matrix material as a result of transverse fiber failure in the subsurface axial fiber tows. The surface strain at the time fiber splitting occurs can be determined by plotting the global stress versus local strain curve at the split locations. Figure 9 shows four such curves along with the four point locations for the T700S/PR520 material. The surface strain field is shown when the global strain is 1.57%.

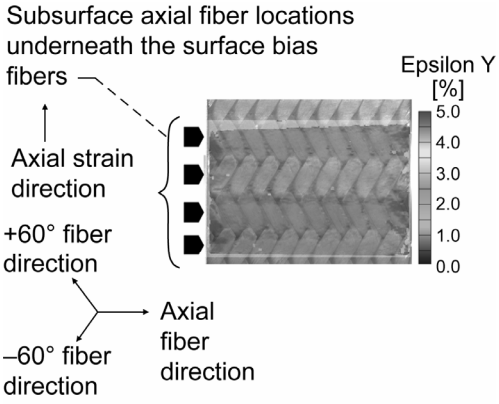

Figure 7. Overlay of axial strain on a representative transverse tension specimen.

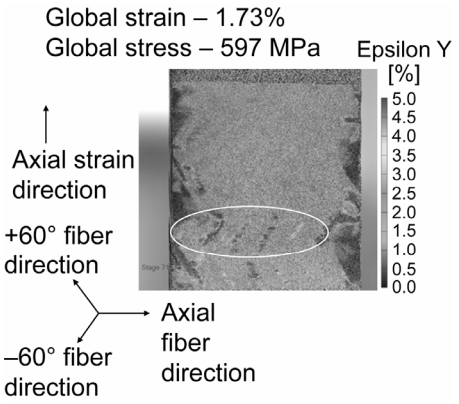

Figure 8. Example of fiber bundle splitting in the T700s fiber/PR520 resin material system.

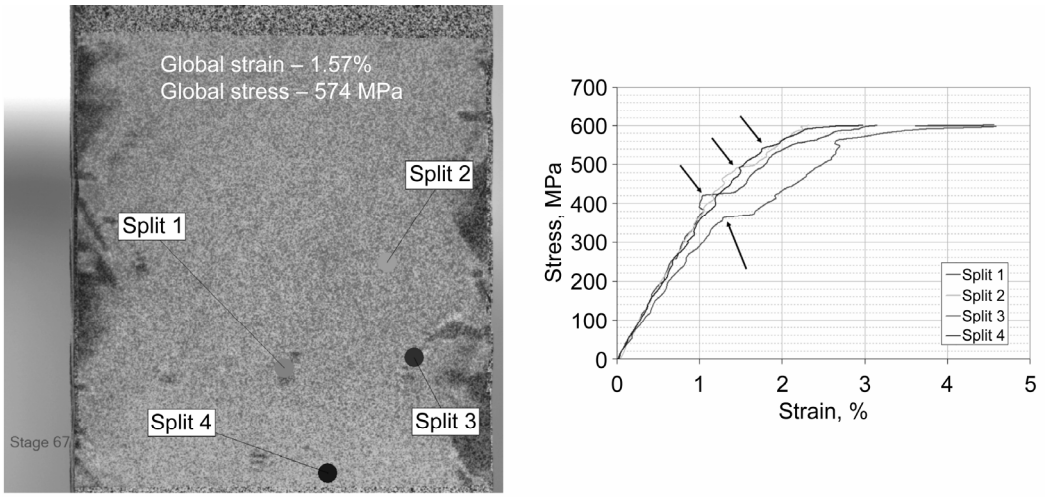

Figure 9. Example fiber bundle/matrix system splitting for T700s fiber/PR520 resin material system.

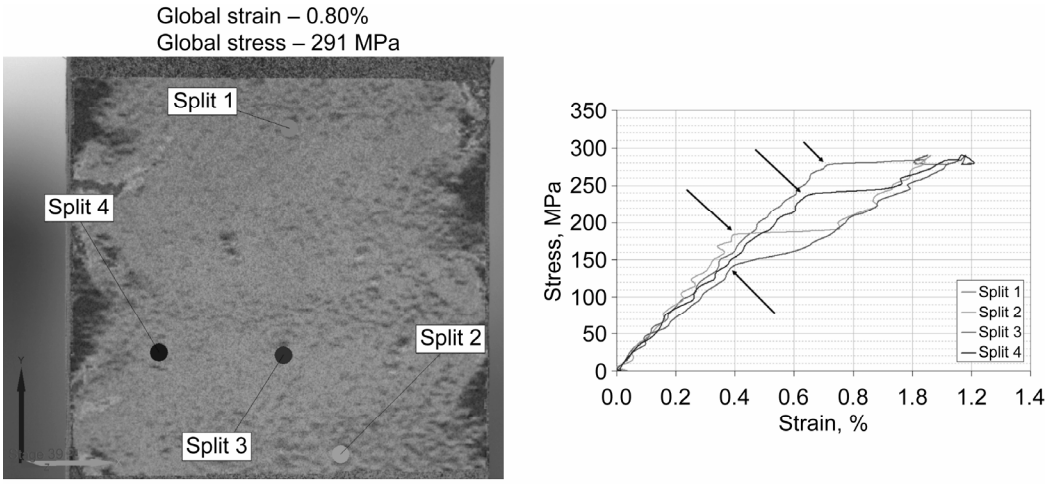

Figure 10. Example fiber bundle/matrix system splitting for T700s fiber/5208 resin material system.

A split appears as a sharp increase in strain at some specific load in the stress-strain curve. For example, in Figure 9 the stress-strain curve measured at the location of split #3 shows a sharp increase in strain at a load of about 360 MPa. For the four curves shown in Figure 9, splitting occurs at surface strains ranging from about 1.0 to1.8%.

Similar to the discussion above, this information is useful for materials evaluation and also provides in-situ material failure properties that could be used in analysis. Figure 10 shows data similar to that in Figure 9 except that the material is T700S/5208 and the global strain for the picture is 0.80%.

For the four curves shown in Figure 10, splitting occurs at surface strains ranging from about 0.4 to 0.7%, which is lower than in the T700s fiber / PR520 resin material system. The accumulation of local failures of the type evident in Figures 9 and 10 contributes to the nonlinearity of the global transverse tensile curves shown in Figures 3 and 4. During the transverse tensile test, axial fiber bundles split over a range of strains when the local transverse strength is exceeded, but the composite fails at the global failure strain. Between the initiation of fiber bundle splitting and global composite failure, the fiber bundle splits are initiating and propagating throughout the

composite, representing damage accumulation. Once damage accumulation reaches a critical value, the composite fails.

Also shown in Figures 8, 9, and 10 are approximately triangular areas of low strain represented by dark blue sections along the free edges of the specimens. These damaged edge regions were observed only in the transverse tensile tests. Since the damaged edge regions carry little load, the extent of edge damage observed indicates that the global transverse tensile strength measured using a standard straight-sided specimen could be significantly lower than the actual strength of the material in a structure since material embedded within the structure would not have such edge effects. The occurrence of this edge damage in the test specimen is probably a result of how the bias fibers terminate at the free edges. In the axial tensile test specimen bias fibers at the edge of the specimen are bonded to axial fibers that extend completely between the gripped ends of the specimen. These axial fibers do not fail until the strain approaches the global failure strain, and the bias fibers do not appear to locally debond from the axial fibers. In the transverse tensile test specimen the bias fibers are bonded to axial tows in the braid that are being loaded transverse to the axial fiber direction. Local failure occurs as a result of the weak transverse strength of the fiber tows. Alternative specimens designs have been proposed to eliminate this deficiency in the transverse tensile test when used on large unit cell size braided composites. One alternative is a "bowtie" specimen geometry (Bowman 2003), in which all of the axial and bias fibers in the gage section are gripped during the test. The other is a tubular specimen geometry, in which axial and bias fiber bundles extend along the entire specimen length. Future work is planned to examine the relative merits and deficiencies of alternative specimen designs.

Effect of matrix material

The results presented above indicate that the onset of local failure is lower for T700S/5208 versus T700S/PR520. Since the local failures are primarily fiber bundle splits, a lower transverse fiber failure strain could result from either a weaker resin material or a weaker fiber/matrix interface strength. The fiber/matrix properties were not measured in this work, but the difference between the two material systems is consistent with the matrix strength values indicated in Table 2. To more closely examine the difference between materials, a sequence of images is shown in Figure 11 showing the evolution of damage. Results are shown for the axial tensile test rather than the transverse tensile test to avoid the complications of edge damage discussed above for the transverse tensile test. The three images for each material represent the onset of fiber bundle splitting, fiber bundle splitting at a common intermediate stress, and the extent of fiber bundle splitting at the last data point collected before failure.

The onset of fiber splitting occurs at a much lower strain for the untoughened T700S/5208 material compared to the toughened T700S/PR520 material. At nearly equal intermediate loads the untoughened material has much more fiber splitting. Near failure the untoughened material has extensive fiber splitting while the toughened material has just a few splits per tow. For the T700S/PR520 material the global failure strain of 2.21% is nearly the same as the failure strain for the fiber alone. The splits in the bias fibers do not prevent the axial fibers from being fully loaded prior to failure. For the T700S/5208 material the global failure strain of 1.57% is much lower than the failure strain for the fiber alone. If the splitting of the bias

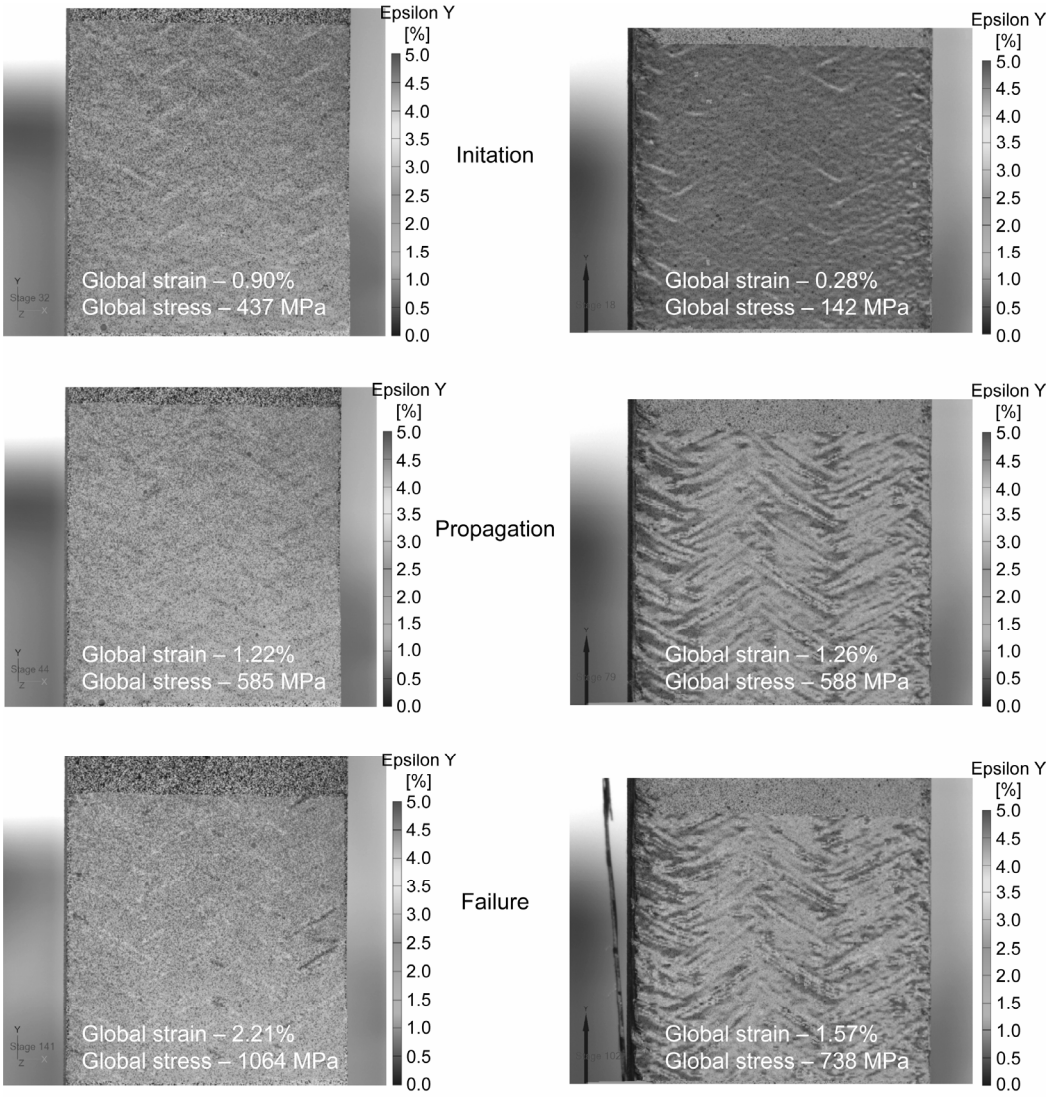

Figure 11. Axial strain time histories of T700s/PR520 (left) and T700s/5208 (right).

fibers resulted only in reduced strength within the bias fiber bundles, the global strength would decrease, but the axial fibers would still carry load until the global strain reached the fiber failure strain of about 2.2%. Since the composite fails at a global strain of 1.57%, splits in the bias fibers must act as local stress concentrations causing premature failure of the axial fibers. The digital image correlation method is a powerful and efficient tool for investigating these matrix effects.

Conclusions

Digital image correlation and image processing techniques were developed to investigate the deformation and failure of large unit cell size triaxial braid carbon fiber composites. The initiation and growth of fiber splits in the surface bias fibers and the subsurface axial fibers were the primary local failure modes observed. Overlay techniques were developed so that the location of local stress concentrations could be mapped onto an image of the composite surface. Quantitative values for local failure strain could be determined by measuring the local strain history at the site of a split and plotting the global stress versus local strain curve. Data obtained using

these new methods provided insight into the mechanisms that control global strength for composites made with untoughened and toughened matrix materials. Splits within fiber tows of the untoughened material appeared to act as local stress concentrations that limited the strain capability of axial fibers. There were fewer fiber splits within tows of the toughened fiber, and these splits did not limit the ability of axial tows to achieve their full strain capability before failure. Results from the full field strain measurements indicated potential problems with the use of standard straight-sided test specimens for measuring transverse strength of large unit cell size braided composites because of edge effects. The optical techniques reported in this paper provide an efficient method for investigating local failure phenomena in large unit cell size triaxial braid. A large amount of information can be obtained from a single test rather than using multiple tests interrupted at various strain levels followed by microscopic examination.

References

ASTM D 3039. (2006) "Standard Test Method for Tensile Properties of Polymer Matrix Composite Materials."

Bowman, C.L. et al. (2003) "Mechanical Properties of Triaxial Braided Carbon/Epoxy Composites." NASA/TM 20030113144.

Composite Materials Handbook 17 Volume 1. (2002) "Polymer Matrix Composites Guidelines for Characterization of Structural Materials." MIL-HDBK-17-1F.

Federal Aviation Administration. (2003) "Material Qualification and Equivalency for Polymer Matrix composite Material Systems: Updated Procedure." DOT/FAA/AR-03/19.

Gliesche, Konrad et al. (2005) "Investigations of in-plane shear properties of ±45° carbon/epoxy composite using tensile testing and optical deformation analysis." Composites Science and Technology 65.

GOM Optical Measurement Techniques. www.gom.com Accessed Jan 11, 2008.

Littell, J.D., et al. "Measurement of Epoxy Resin Tension, Compression, and Shear Stress-Strain Curves Over a Wide Range of Strain Rates and Temperatures." J. of Aerospace Eng. Sp. Issue – "Impact Mechanics and High Energy Absorption Materials." Accepted, In Publication.

Masters, John E. et al. (1993) "The Effects of Specimen Width on Tensile Properties of Triaxially Braided Textile Composites." NASA TM 19950022404.

Masters, John E. (Feb. 1996) "Strain Gage Selection Criteria for Textile Composites." NASA CR 198286.

Masters, John E. and Portanova, Marc A. (Sept. 1996) "Standard Test Methods of Textile Composites." NASA CR 4751.

Masters, John E. and Ifju, Peter G. (1996) "A Phenomenological Study of Triaxially Braided Textile Composites Loaded in Tension." Composites Science and Technology 56 (347–358).

Tomblin, J. Abbott, R., and Stenard, S. (2001) "Material Qualification Methodology for 2X2 Biaxaially Braided RTM Composite Material Systems." AGATE-WP3.3-033048-116.

Tsotsis, T.K. et al. (2006) "Towards Rapid Screening of New Composite Matrix Resins." Composites Science and Technology 66.